Impurity accumulation spectroscopically observed during ion cyclotron resonance frequency heating experiments in the JIPP T-II-U tokamak

K. Ono, T. Oomori, and Y. Ueda*
Central Research Laboratory, Mitsubishi Electric Corporation, Tsukaguchi-honmachi, Amagasaki 661, Japan

K. Sato, K. Toi, T. Watari, I. Ogawa, K. Kawahata, R. Ando,
Y. Kawasumi, N. Noda, and S. Tanahashi
Institute of Plasma Physics, Nagoya University, Chikusa-ku, Nagoya 464, Japan
(Received 21 February 1986)

Spectroscopic investigations of iron-ion line radiation (Fe X–XXIV) in the extreme-ultraviolet region have been carried out during ion cyclotron resonance frequency (ICRF) heating experiments in the JIPP T-II-U tokamak, at the Japanese Institute of Plasma Physics (JIPP), Nagoya University, Nagoya. The central-chord radiances of the iron-ion resonance lines were observed to increase during ICRF heating. After the radiance of the highest ionization stage attained the peak toward the end of ICRF heating, the radiances of the lower stages were observed to attain their peaks at successively later times. The rf-power injection was accompanied by strong gas puffing and additional current rise, which raised the electron density and concurrently lowered the central electron-temperature. The electron-temperature decrease in the central region, which was further promoted by radiative losses due to metallic impurities, continued after ICRF heating. The spectroscopic observations are interpreted as showing that the ICRF heating causes a large additional influx of iron into the plasma, and that the iron accumulates preferentially in the plasma interior with long confinement times. The sequential peaking of the radiation from the highest to the lowest ionization stages reflects the decrease in the electron temperature and the concurrent recombination into successively lower stages. These interpretations are supported by the soft-x-ray and bolometric measurements, and confirmed by the modeling calculations that reproduce the iron-ion line radiances.

I. INTRODUCTION

Impurity effects still constitute one of the most important problems in tokamak plasmas.[1] Impurities can adversely affect the overall energy confinement and the local power balance of such plasmas, through their line radiation and their contribution to the plasma resistivity. In recent years these impurity effects have been considerably reduced; relatively pure plasmas are currently obtained in all tokamaks by various impurity control techniques such as discharge cleaning, titanium gettering, use of graphite limiters, and precise plasma-position control. Nevertheless, the typical influxes of metallic impurities encountered in many tokamaks would be unacceptable if the impurities accumulated preferentially in the interior of the plasma. Interior accumulation of metallic impurities leads to plasma disruptions or to excessive radiation losses in the plasma interior. Such impurity accumulation, predicted to occur from neoclassical transport theory, has been observed in some tokamak experiments with Ohmic heating only[2–7] and with auxiliary heating by neutral-beam injection (NBI).[6,8–11] However, it has been generally possible to operate the tokamak in such a way that no accumulation occurs. Anomalous transport is often invoked to explain this lack of accumulation.

As a means of auxiliary heating alternative to NBI, ion cyclotron resonance frequency (ICRF) heating has been recently carried out in a number of tokamak experiments. In earlier experiments with ICRF heating where intermediate-Z metals were used for limiters,[12,13] the levels of metallic impurities were so high that central radiated power densities reached a level comparable to the ICRF heating power density; in some cases,[13] the plasma interior started to cool during ICRF heating and then disruptions occurred. In more recent ICRF heating experiments with low-Z graphite limiters,[14–20] the metallic impurity concentrations have been considerably reduced; currently, the central radiation losses do not play a major role in the discharge power balance and the heating efficiency is not affected substantially. However, the levels of metallic impurities are still higher during ICRF heating than during Ohmic heating or NBI at similar power levels. In general, auxiliary heating tends to strongly enhance metallic impurity generation at internal structures such as walls, limiters, and antennas, leading to large additional influxes of such impurities which then penetrate to the plasma interior. So far, a great deal of attention has been focused on the source and its rates of metallic impurities during ICRF heating; however, their rapid penetration to the plasma interior has not come into question.

In this paper, we describe and analyze spectroscopic observations of iron-ion line radiation in the extreme-ultraviolet (xuv) region during ICRF heating experiments in the JIPP T-II-U tokamak.[18,20] Emphasis is placed on the radiation increase during ICRF heating and on the subsequent sequential peaking of the radiation from the highest to the lowest ionization stages. These observations are interpreted as showing that iron ions accumulate preferentially in the central region of the plasma with

long confinement times. In the present experiments, impurity levels are relatively low and accumulation is not serious; however, the present results emphasize that a deeper understanding of impurity transport and confinement as well as of impurity generation may be needed for near-future tokamak experiments with higher-power, longer-pulse ICRF heating. The next section gives a brief description of the machine, the operation, and the diagnostics used in this study. Section III presents the results of spectroscopic measurements, together with those of soft-x-ray and bolometric ones, for both discharges with and without ICRF heating. Finally, Sec. IV contains modeling calculations that reproduce the iron-ion line radiances measured in the experiments.

II. EXPERIMENTAL ARRANGEMENT

The JIPP T-II-U tokamak was operated with graphite limiters, a nominal minor radius $a=23$ [cm, a nominal major radius $R=91$ cm, a toroidal magnetic field $B_T=26.4$—30.0 kG, and stainless-steel walls. Typical plasma parameters during the quasisteady part of the Ohmically heated discharges were the following: working gas D_2 with 3—20% H_2 minority, plasma current $I_p=170$ kA, line-average electron density $\bar{n}_e\approx 2\times 10^{13}$ cm^{-3}, central electron density $n_e(0)\approx 3\times 10^{13} cm^{-3}$, central electron temperature $T_e(0)\approx 1$ keV, and central ion temperature $T_i(0)\approx 0.5$ keV. In the JIPP T-II-U ICRF heating experiments, rf-power injection was accompanied by strong gas puffing and additional current rise, in order to suppress impurity influxes and growth of $m=2$ magnetohydrodynamic (MHD) activity.[18,20] Strong puffing of the working gas was initiated at 100 ms during the above quasisteady discharge condition, and the gas was continuously bled into the discharge until 140 ms; additional current rise was initiated at 117 ms, and the current was increased up to $I_{pm}=240$—290 kA in about 25 ms. Then ICRF heating in the H minority regime was carried out between 118 and 153 ms at an rf power $P_{rf}=500$—800 kW (exceeding the Ohmic power input $P_{Ohmic}\approx 300$ kW) having the 40 MHz frequency. Two of the three ICRF antennas had stainless-steel Faraday shields, and the remaining one had titanium Faraday shields.

Spectral line emission intensities in the xuv region, 30—1100Å, were measured with a 2-m grazing-incidence monochromator and a CsI-cathode electron multiplier. The wavelength resolution was about 0.2 Å, and the line of sight was along a chord through the center of the plasma. The sensitivity of this monochromator system was relatively calibrated over the entire wavelength range and absolutely calibrated at two wavelengths of the H L_β and L_γ lines by the branching-ratio technique.[21] The line-average electron density along the central chord was measured by microwave interferometry, and the central electron temperature from second-harmonic electron cyclotron emission. The radial profiles of electron density and temperature were measured by ruby-laser Thomson scattering. The near-central ion temperature was measured from the charge-exchanged D^0 energy distribution. The energy emitted from the plasma, consisting of photons mostly in the xuv region and charge-exchanged neutral atoms, was measured with an array of bolometers viewing different chords. The soft-x-ray emission at photon energies above 1 keV was monitored with an array of silicon detectors viewing different chords.

III. EXPERIMENTAL RESULTS AND INTERPRETATIONS

Figures 1(a)—4(a) show typical results for the Ohmically heated discharges including strong gas puffing and additional current rise. These data provide a reference for later comparison with the results obtained when ICRF heating was carried out. Figure 1(a) shows the time evolution of the plasma current I_p, the line-average electron density $\bar{n}_e$, the central electron density $n_e(0)$, and the central electron temperature $T_e(0)$ for a D_2 discharge with 3% H_2 minority, $B_T=28.8$ kG, and $I_{pm}=240$ kA. The density increases from $\bar{n}_e\approx 2\times 10^{13}$ to 6×10^{13} cm^{-3} in about 60 ms after the initiation of gas puffing at 100 ms. The density profile was slightly hollow with the maximum at $r\approx 7$ cm during the steep part of the density increase. The central electron temperature reaches the maximum value $T_e(0)\approx 1.4$ keV at about 120 ms, and then decreases to $T_e(0)\approx 1$ keV during the density increase. However, the electron temperature remained almost unchanged at intermediate radii, so that the centrally peaked

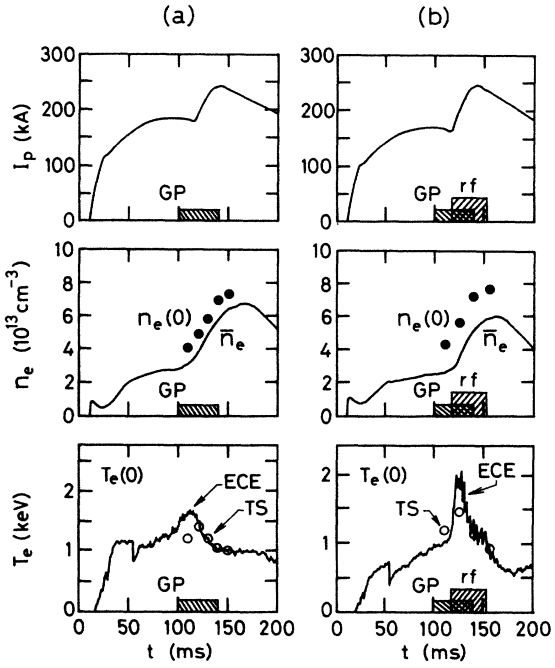

FIG. 1. Time evolutions of the plasma current I_p, the line-average electron density $\bar{n}_e$, the central electron density $n_e(0)$, and the central electron temperature $T_e(0)$ for JIPP T-II-U discharges (a) with Ohmic heating only and (b) with ICRF heating; $T_e(0)$ was measured by Thomson scattering (TS) and from second-harmonic electron cyclotron emission (ECE). These discharges include strong gas puffing (GP) and additional current rise; in (b), ICRF heating (rf) lasts 35 ms from 118 to 153 ms. Discharge conditions: working gas D_2 with 3% H_2 minority, $B_T=28.8$ kG, $I_{pm}=240$ kA, and $P_{rf}=500$ kW.

profile of the electron temperature flattened gradually inside $r \approx 7$ cm after about 120 ms. The central ion temperature fell by about 50 eV after about 120 ms during the density increase, and thereafter returned to its initial level.

Figure 2(a) shows the time evolution of the emission intensities of several iron-ion resonance lines for the Ohmically heated discharge of Fig. 1(a). These signals are central-chord radiances. The Fe XXIII resonance line at 132.83 Å overlaps with a Fe XX resonance line at 132.85 Å. The Fe XX 132-Å line intensity is estimated to be about twice as large as the Fe XX 118-Å line intensity. In this estimation, the Boltzmann distribution is assumed between upper-level populations of the two Fe XX resonance transitions, and the atomic data are taken from the tables of Fuhr *et al.*[22] Thus, around 120 ms when the Fe XXIII signal attains the peak, about half of the Fe XXIII 132-Å signal is a contribution from Fe XX; in the early and late parts of the discharge, however, most of it is a contribution from Fe XX. Between the start of the discharge and about 120 ms, higher ionization stages are seen to appear and attain peak intensities at successively later times. Each line intensity drops after reaching its own peak. The high ionization stages Fe XX–XXIV, which radiate in the central region of the plasma, attain their peak intensities after the initiation of gas puffing at 100 ms. This is consistent with the result that the central electron temperature does not decrease until about 20 ms after the initiation of gas puffing.

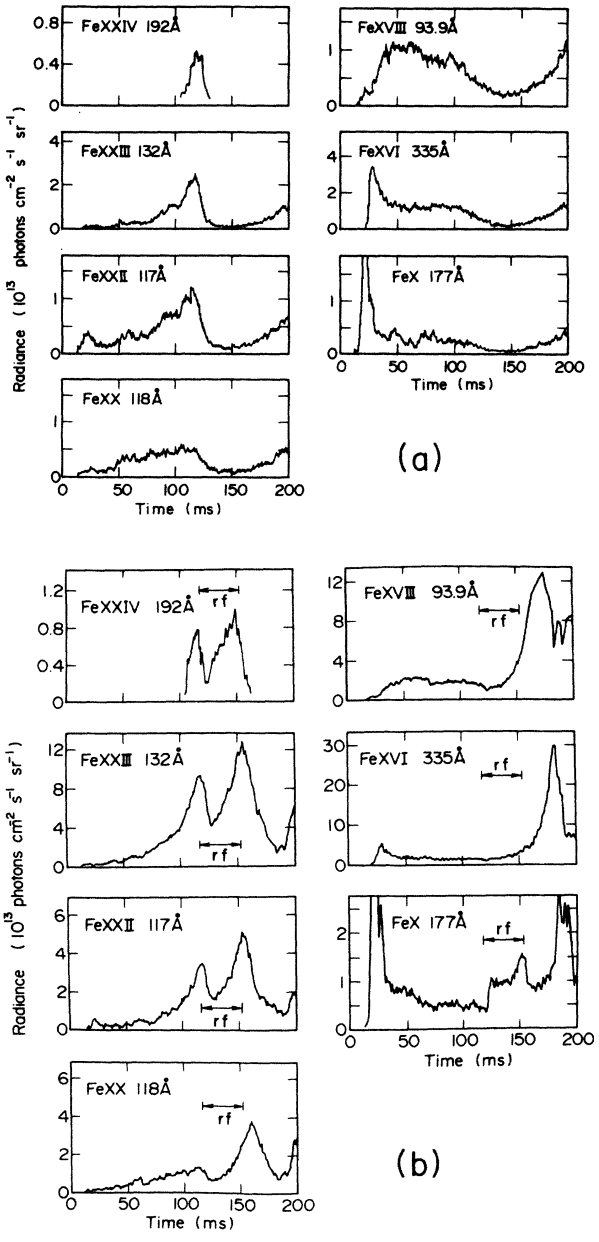

FIG. 2. Time evolutions of the central-chord radiances of several iron-ion resonance lines for (a) the Ohmically heated and (b) the ICRF heated discharges of Fig. 1. The Fe XXIII 132-Å signal includes a contribution from Fe XX, owing to the blending of the Fe XXIII 132.83-Å and Fe XX 132.85-Å lines.

All the line intensities show a substantial drop during gas puffing, in spite of the increasing electron density, indicating a large decrease of the iron concentration. This intensity drop is more noticeable in the higher ionization stages. Such a substantial drop in metallic impurity line intensities due to gas puffing has been observed in a number of tokamak experiments;[23–27] the intensity drop has been ascribed mostly to a large decrease of the metallic impurity concentrations in the discharge following the lowering of the peripheral electron temperature. Gas puffing raises the electron density and concurrently lowers the electron temperature, since the energy content of a plasma remains almost unchanged by this operation. The lowered temperature at the plasma periphery leads to reduced impurity generation at the limiters and walls, resulting in reduced impurity influxes into the plasma. The larger intensity drop in the higher ionization stages has been ascribed to a lowering of the electron temperature with consequent changes in the ionization balance. A more detailed account of the spectroscopic observations in this type of discharge will appear in another paper.[20]

Figures 1(b)–4(b) show typical results from the ICRF heating experiments, where ICRF heating at $P_{rf} = 500$ kW was applied to the Ohmically heated discharge of Figs. 1(a)–4(a) between 118 and 153 ms. Figure 1(b) shows the time evolution of the same plasma parameters as shown in Fig. 1(a). It is natural that the time evolutions of the plasma condition are almost the same in the two cases with Ohmic heating only and with ICRF heating at least up to 118 ms when the ICRF heating is initiated. The evolutions of the plasma current I_p, the line-average electron density $\bar{n}_e$, and the central electron density $n_e(0)$ are very similar in both cases during the whole period of the discharge. The density profiles were also similar in both cases. It is therefore evident that the ICRF heating itself makes no appreciable contribution to the density increase; the density increases by about a factor of 3 in about 60 ms owing to the strong gas puffing initiated at 100 ms.

The time evolution of the electron and ion temperatures in the ICRF heating case differs markedly from that in the Ohmic heating one. The central electron temperature increases rapidly to $T_e(0) \approx 1.8$ keV within about 5 ms after the initiation of ICRF heating, because the ICRF power can be coupled with electrons as well as ions.[28]

However, the central electron temperature begins to decrease at about 125 ms during ICRF heating; it decreases to $T_e(0) \approx 0.5$ keV in about 50 ms during and after ICRF heating. This decreasing rate of $T_e(0)$ is much faster than that in the Ohmic heating case where the decrease in $T_e(0)$ is ascribed mostly to the density increase due to gas puffing. The electron temperature continued increasing or remained almost unchanged at intermediate radii, in spite of the rapid decrease in $T_e(0)$; consequently, the centrally peaked profile of the electron temperature flattened rapidly after about 125 ms, leading to a slightly hollow profile with the maximum at $r \approx 7-10$ cm around 155 ms. Such hollow temperature profiles have been observed in some tokamak experiments,[9,11,24,29] and are now known to be caused by large radiative losses due to metallic impurities in the central region of the plasma. It is therefore probable that the rapid decrease in $T_e(0)$ during and after ICRF heating is attributable both to gas puffing and to radiative losses. The signal of the electron cyclotron emission shows a large sawtooth oscillation during ICRF heating. The central ion temperature rose by $\Delta T_i(0) \approx 0.5$ keV during ICRF heating, and thereafter returned to its initial level. The ion heating efficiency is relatively high:

$$\Delta T_i(0)\bar{n}_e / P_{\mathrm{rf}} \approx (3-6) \times 10^{13}\ \mathrm{eV\,cm^{-3}\,kW^{-1}}\ .$$

Figure 2(b) shows the time evolution of the iron-ion line intensities for the ICRF heated discharge of Fig. 1(b). These signals are central-chord radiances of the same spectral lines as shown in Fig. 2(a) for the Ohmic heating case. The evolutions of the emission intensity of each line are very similar in both cases up to about 120–125 ms, about 2–7 ms after the initiation of ICRF heating, aside from the difference in the absolute radiance. The absolute line radiances depend on the discharge conditions and the condition of the vacuum vessel; the data in Figs. 2(a) and 2(b) were obtained at separate days during a long series of experiments. All the line intensities show a substantial drop due to the gas puffing initiated at 100 ms. After this drop, which is more noticeable in the higher ionization stages, the evolution of the line intensities in the ICRF heating case differs strikingly from that in the Ohmic heating one. The line intensity of the low ionization stage Fe X, which radiates near the edge of the plasma, rises by about a factor of 2–3 after about 120 ms during ICRF heating, and thereafter returns to its slowly rising base level. This result indicates a large additional influx of iron into the plasma during ICRF heating.

The line intensities of the intermediate and high ionization stages Fe XVI–XXIV, which radiate near the middle and center of the plasma, begin to rise at about 125 ms; they rise by about a factor of 3–4 during ICRF heating. This intensity rise that is much faster than the electron-density increase may, in a sense, be ascribed to a considerable increase of the iron concentration in the discharge due to the additional influx. The line intensities depend on the electron temperature T_e as well as on the electron density and the iron concentration along the spectrometer line of sight. All the iron-ion lines in Fig. 2 originate from $\Delta n = 0$ resonance transition; their excitation rate coefficients by electron impact are practically independent of T_e over the range 0.2–2 keV where the ions exist. Consequently, the line intensities depend on T_e only through the fractional abundances of iron ionization stages. While all the line intensities show a substantial rise after about 125 ms during ICRF heating, the electron temperature decreases from $T_e \approx 1.8$ to 1 keV in the central region where the high ionization stages radiate. This T_e decrease should result in a marked decrease of the abundances of high stages such as Fe XXIV. Therefore, if the iron concentration did not increase preferentially in the central region, but increased at almost the same rate throughout the plasma, the intensity rise during ICRF heating would be less noticeable in the higher ionization stages. This is contrary to the present observations. Preferential accumulation of iron must be taken into account in the central region of the plasma, in order to explain the substantial rise in the line intensities of high ionization stages such as Fe XXIV during ICRF heating.[4,6,8,9,11]

The highest ionization stage Fe XXIV attains the peak intensity at about 150 ms, about 3 ms before the termination of ICRF heating; then the lower stages attain their peak intensities at successively later times while the electron temperature decreases from $T_e \approx 1$ to 0.5 keV in the centrai region. Each line intensity drops after reaching its own peak. This sequential peaking of the emission reflects the decrease in T_e and the concurrent recombination into successively lower stages without substantial changes in the iron concentration.[4,6,8,9,11] If a large decrease of the iron concentration took place in the discharge after ICRF heating, all the line intensities would show a substantial drop without sequential peaking. An influx of iron into the plasma after ICRF heating is probably much smaller than that during ICRF heating. Therefore, it appears that the iron, which has flowed into the plasma and accumulated in its central region during ICRF heating, is retained in the plasma with relatively long confinement times after ICRF heating.

Soft-x-ray and bolometric measurements support the spectroscopic observations on the impurity behavior. Figures 3(a) and 3(b) show the time evolution of the central-chord soft-x-ray emission and the total radiated power

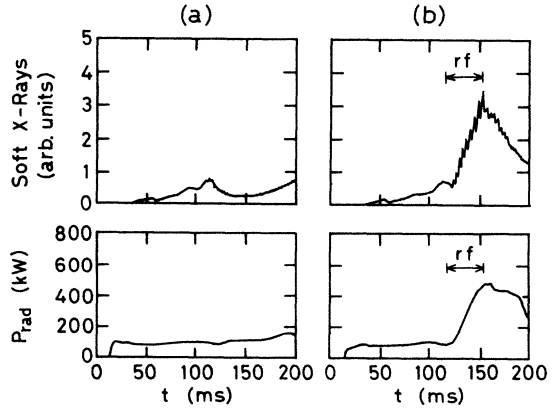

FIG. 3. Time evolutions of the central-chord soft-x-ray emission and the total radiated power P_{rad} for (a) the Ohmically heated and (b) the ICRF heated discharges of Fig. 1.

P_{rad} for the Ohmically and the ICRF heated discharges of Fig. 1, respectively. In each case, the central-chord soft-x-ray signal has a similar time evolution to the signals of the high ionization stages Fe XX–XXIII in Fig. 2; a substantial drop due to gas puffing is seen around 120 ms. The soft-x-ray emission depends on the electron temperature T_e and density n_e, and also on the level of impurities; the T_e dependence is so strong that most of the emission along the detector line of sight tends to be localized where T_e is highest. The central-chord soft-x-ray emission comes mostly from the central region of the plasma. After the drop due to gas puffing, it rises continuously at a rate much faster than the n_e increase during ICRF heating, though T_e is decreasing in the central region. This emission rise was noticeable on all detectors viewing different chords. The soft-x-ray emission drops following the termination of ICRF heating. These results indicate that the impurity levels in the discharge increase considerably during ICRF heating owing to large additional influxes of impurities into the plasma, and that this increase occurs preferentially in the central region. If impurities did not accumulate preferentially in the central region of the plasma, the emission rise during ICRF heating would be less noticeable on detectors viewing the chords nearer to the central one, because of the T_e decrease in the central region. It is also evident that the impurity levels in the discharge do not continue to increase considerably after ICRF heating. The central-chord soft-x-ray signal, together with the signal of the electron cyclotron emission in Fig. 1(b), shows a large sawtooth oscillation during ICRF heating.

Such a substantial rise in the central-chord soft-x-ray emission has been observed in some tokamak experiments,[2,4–8,10] and has been ascribed to central accumulation of metallic impurities. In some cases, the onset of accumulation was accompanied by the disappearance of the sawteeth.[2] Theoretical calculations have also shown that sawtooth oscillations (periodic internal disruptions) can significantly reduce impurity accumulation (impurity confinement times) if inward convection is large enough relative to diffusion in the impurity flux.[30] In some cases,[4,6] however, accumulation took place concurrently with well-defined sawtoothing activity as in the present experiments.

The total radiated power in the Ohmic heating case remains almost constant during the whole period of the discharge; a very little drop due to gas puffing is seen around 120 ms. After this drop, the total radiated power in the ICRF heating case increases continuously from $P_{rad} \approx 100$ to 500 kW during ICRF heating, and thereafter maintains a relatively constant value for about 20–30 ms. The value of P_{rad} toward the end of ICRF heating is nearly equal to the ICRF heating power P_{rf}, corresponding to about 60% of the total input power $P_{tot} = P_{Ohmic} + P_{rf}$ ($P_{Ohmic} \approx 300$ kW, $P_{rf} \approx 500$ kW) to the plasma.

Figures 4(a) and 4(b) show the time evolution of the radial profile of the radiated power density W_{rad} for the Ohmically and the ICRF heated discharges of Fig. 1, respectively. The radiation profile $W_{rad}(r)$ in the Ohmic heating case remains fairly flat between 100 and 170 ms, whereas that in the ICRF heating one evolves toward a centrally peaked profile. In each case, the near-central radiation at $r \lesssim 10$ cm, largely due to metallic impurities, has a similar time evolution to a superposition of the signals of the intermediate and high ionization stages Fe XVI–XXIV in Fig. 2; a substantial drop due to gas puffing is seen around 120 ms. After this drop, which is more noticeable at smaller radii, the near-central radiation increases gradually during ICRF heating without appreciable profile modifications. The values of $W_{rad}(r)$ within $r \approx 10$ cm toward the end of ICRF heating are comparable to or exceeding the volume-average density $\overline{W}_{tot} \approx 0.85$ W cm^{-3} of the total input power P_{tot}. After ICRF heating, the near-central radiation increases continuously at a rate much faster than it does during ICRF heating. This increase is more noticeable at smaller radii, leading to a centrally peaked radiation profile. It is probable, near the center of the plasma during and after ICRF heating, that the radiative losses are not small enough to be negligible in the discharge power balance, being responsible for the rapid decrease in the electron temperature as seen in Fig. 1(b).

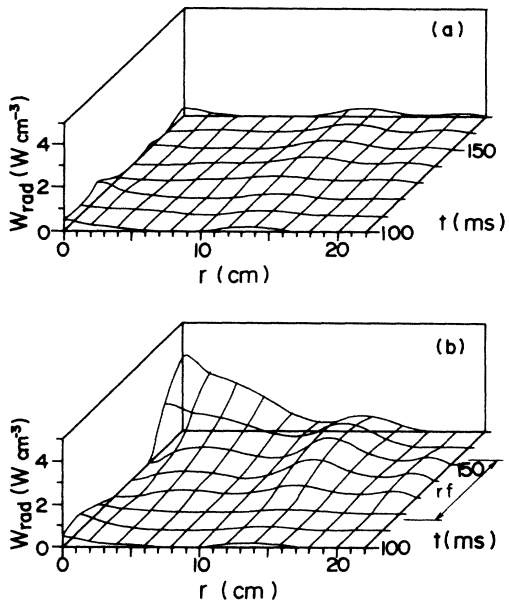

FIG. 4. Time evolutions of the radial profile of the radiated power density W_{rad} for (a) the Ohmically heated and (b) the ICRF heated discharges of Fig. 1.

Central accumulation of metallic impurities that has been observed so far in tokamak experiments usually ended in plasma disruptions following excessive radiation losses in the central region of the plasma.[9,10] This cause-and-effect relationship is not clearly established in the present experiments, however. The present accumulation, which takes place during ICRF heating as indicated by the spectroscopic and soft-x-ray data in Figs. 2(b) and 3(b), does not lead even to excessive radiation losses in the central region; the radiation profile $W_{rad}(r)$ is not centrally peaked during ICRF heating. This may be ascribed to the low level of metallic impurities in the discharge. The metallic impurity concentrations are reduced with graph-

ite limiters, and further reduced as a result of strong gas puffing and additional current rise. Following the initiation of ICRF heating, the impurity concentrations in the discharge increase progressively owing to large additional influxes of impurities which are then transported to the central region of the plasma. The profile $W_{rad}(r)$ eventually becomes centrally peaked toward the end of ICRF heating, and thereafter becomes more and more centrally peaked.

Neither substantial increase nor decrease of impurity concentrations takes place in the discharge after ICRF heating, as indicated by the spectroscopic and soft-x-ray data in Figs. 2(b) and 3(b). The substantial increase in the near-central radiation after ICRF heating is consistent with the sequential peaking of the emission from the highest to the lowest ionization stages of iron as seen in Fig. 2(b); this radiation increase is probably related to an increase of the radiation efficiencies of impurities with decreasing electron temperature.[31,32]

The data in Figs. 1–4 are the results for D_2 discharges with 3% H_2 minority, toroidal magnetic field $B_T=28.8$ kG, maximum plasma current $I_{pm}=240$ kA, and ICRF heating power $P_{rf}=500$ kW. Similar results were obtained for the following wide range of discharge conditions: working gas D_2 with 3–20 % H_2 minority, $B_T=26.4$–30.0 kG, $I_{pm}=240$–290 kA, and $P_{rf}=500$–800 kW.

IV. DISCUSSION AND CONCLUSIONS

In the present ICRF heating experiments with strong gas puffing and additional current rise, the evidence for preferential accumulation of intrinsic iron in the central region of the plasma is essentially as follows: the line intensities of high ionization stages such as Fe XXIV rise substantially during ICRF heating [Fig. 2(b)], though the electron temperature is decreasing in the central region where the high stages radiate [Fig. 1(b)]. This intensity rise is much faster than the electron-density increase [Fig. 1(b)]. The iron concentration in the discharge increases considerably during ICRF heating owing to a large additional influx of iron into the plasma, as indicated by a substantial rise in all the line intensities of different ionization stages [Fig. 2(b)]. However, the electron-temperature decrease in the central region should result in a marked decrease of the fractional abundances of high ionization stages such as Fe XXIV. Therefore, if the iron concentration did not increase preferentially in the central region, but increased at almost the same rate throughout the plasma, the intensity rise during ICRF heating would be less noticeable in the higher ionization stages.

Recent measurements of soft-x-ray spectra in the present discharges have shown that Fe XXV is scarcely produced, i.e., Fe XXIV is the terminal stage of ionization.[33] After the highest ionization stage Fe XXIV attains the peak intensity toward the end of ICRF heating, the lower stages attain their peak intensities at successively later times [Fig. 2(b)]; each line intensity drops after reaching its own peak. This sequential peaking of the emission reflects the decrease in the electron temperature [Fig. 1(b)] and the concurrent recombination into successively lower stages without substantial changes in the iron concentration. It appears that the iron, which has flowed into the plasma and accumulated in its central region during ICRF heating, is retained in the plasma with relatively long confinement times after ICRF heating.

Similar features of impurity line radiation have been observed in ISX-*B* (Impurity Study Experiment—*B* tokamak at Oak Ridge National Laboratory) discharges with Ohmic heating only[4,6] and with counter-NBI,[6,8,9,11] for intrinsic titanium and iron and for silicon, argon, and titanium introduced as tracer elements. Substantial increases in the central-chord line radiances appeared first in the highest ionization stages and later showed up in the lower stages, while the plasma interior cooled rapidly. These effects were particularly clear in the counter-NBI discharges. Recombination does not explain the radiation increase in the highest ionization stages. The ISX-*B* group has insisted, as in the present paper, that impurity accumulation and long confinement times must be taken into account in order to explain their experimental observations. In PLT (Princeton Large Torus) discharges with counter-NBI and with co-NBI where significant amounts of molybdenum were injected,[34] the line radiances of low ionization stages were observed to increase with time as the plasma interior cooled and the ionization balance changed. In TFR (Tokamak de Fontenay-aux-Roses) discharges the line radiances of different ionization stages of intrinsic nickel were observed to increase during ICRF heating.[13] Following the start of plasma interior cooling toward the end of ICRF heating, the radiance of the highest ionization stage began to decrease and then a disruption occurred. It was indicated that the metallic impurity concentrations in the discharge increased as the ICRF heating caused strong influxes of such impurities which in turn penetrated to the plasma interior.

The evidence for central accumulation of iron in the present ICRF heating experiments is further reinforced by comparing the experimental results with the predictions of time-dependent modeling calculations as described in Refs. 35–37. The comparison is made between the measured and calculated central-chord radiances of the iron-ion resonance lines in Fig. 2. The calculations treat a set of coupled one-dimensional continuity equations for all the ionization stages of iron which include transport as well as ionization and recombination. Cylindrical symmetry is assumed in the calculations; r represents the minor radial coordinate of the toroidal tokamak plasma. The radial flux density Γ_Z of the iron ions of charge Z is taken to have the form $\Gamma_Z=-D_A\partial n_Z/\partial r-(r/a)V_A n_Z$, where n_z is the iron-ion density of charge Z, and a is the minor radius of the plasma. The diffusion coefficient D_A and the inward convection velocity V_A are two adjustable transport parameters independent of radius r and ion charge Z.

The ionization rate coefficients are given by Lotz's formula with his values for the subshell binding energies.[38] The contribution of autoionization to the total ionization rate is taken into account for Fe XVI and XV, according to the calculations of Cowan and Mann.[39] The radiative recombination rate coefficients are given by the modification of the formula for H-like ions proposed by von

Goeler *et al.*[40] The dielectronic recombination rate coefficients are given by Burgess's formula,[41] where two resonance transitions of the recombining ion are considered, the atomic data being taken from the tables of Breton *et al.*[32] For ions less ionized than the Ar-like sequence, two resonance transitions, a $\Delta n=0$ and a $\Delta n=1$, are taken into account, the atomic parameters being calculated with the formulas used by Post *et al.*[31]

The boundary conditions imposed are $(\partial n_Z/\partial r)_{r=0,t}=0$ and $n_Z(a,t)=0$, where $a=23$ cm is the limiter radius. The scrape-off-layer plasma is not considered. It is assumed that iron ions leaving the plasma at $r=a$ are not recycled, and that the iron coming from the walls enters the plasma at $r=a$ as neutral atoms with a constant inward velocity V_0. The incoming neutral atoms are ionized in a narrow shell just inside $r=a$, so that the influx of neutral atoms into the plasma is accounted for by taking their quasisteady density distribution $n_0(r)$ with the inward flux density $n_0(r)V_0$.[26,35] The incoming neutral-iron flux density Γ_0 at $r=a$, $\Gamma_0=n_0(a)V_0$, is the third adjustable parameter in the calculations. The velocity V_0, is taken to be 10^5 cm s^{-1}, corresponding to the neutral-iron kinetic energy of 0.29 eV.

Given the radial profiles of the electron density n_e and temperature T_e, the coupled continuity equations are solved numerically for $n_Z(r,t)$ with the chosen values of D_A, V_A, and Γ_0. The time-dependent functional forms of $n_e(r)$ and $T_e(r)$, determined on the basis of the experimental measurements by Thomson scattering, are employed as input to the calculations. Figure 5 shows the input radial profiles $n_e(r)$ and $T_e(r)$ at various times which have the features described in Sec. III with regard to Fig. 1(b). Here the electron density and temperature at the edge of the plasma were taken as $n_e(a)=0.1n_e(0)$ and $T_e(a)=20$ eV. No measurements of $n_e(r)$ and $T_e(r)$ were done after 155 ms; the relative density profile $[n_e(r)-n_e(a)]/[n_e(0)-n_e(a)]$ was assumed to change gradually to the form $[1-(r/a)^2]$ in 10 ms after 155 ms and then remain unchanged, with the value of the line-average density $\bar{n}_e$ measured by microwave interferometry; the relative temperature profile $[T_e(r)-T_e(a)]/[T_e(0)-T_e(a)]$ was assumed to remain unchanged after 155 ms, with the value of $T_e(0)$ measured from second-harmonic electron cyclotron emission.

The calculations are started at $t=118$ ms, the time of the initiation of ICRF heating which lasts 35 ms from 118 to 153 ms. The iron is initially distributed among different ionization stages as in coronal ionization equilibrium, the total iron density n_{Fe} being taken as $n_{\mathrm{Fe}}(r)=10^{-5}n_e(r)$. The results of the calculations at the time of the experimental measurements concerned, $t\gtrsim 130$ ms, are insensitive to the initial ionization-stage distribution. Once the iron-ion densities $n_Z(r,t)$ have been obtained, the radiances of the iron-ion resonance lines concerned, originating from $\Delta n=0$ transition, are calculated by assuming coronal population equilibrium: the upper level of the transition is populated by electron-impact excitation from the ground level, and is depopulated by spontaneous radiative decay. The electron-impact excitation rate coefficients are given by the formula for optically allowed transitions suggested by Van Regemorter,[42] with the interpolation formula for the effective Gaunt factor proposed by Mewe.[43] The atomic data are taken from the tables of Fuhr *et al.*,[22] including the radiative transition probabilities.

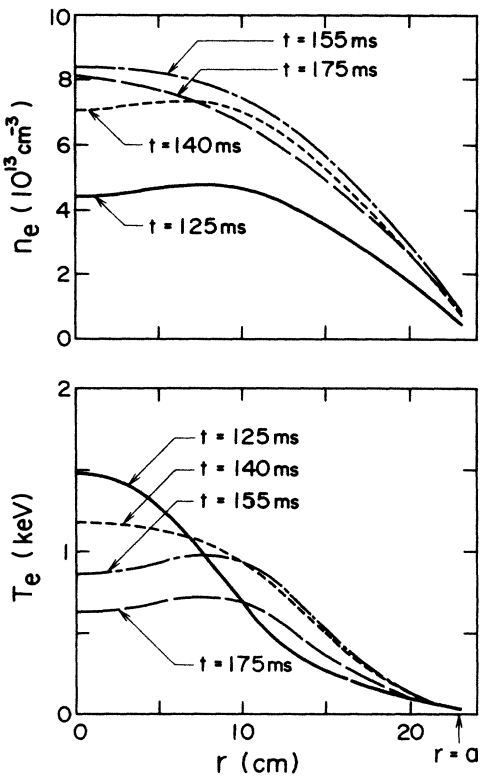

FIG. 5. Input radial profiles of the electron density n_e and temperature T_e at various times. Here $a=23$ cm is the limiter radius. The time-dependent functional forms of $n_e(r)$ and $T_e(r)$, determined on the basis of the experimental measurements by Thomson scattering for the ICRF heated discharge of Fig. 1(b), are employed as input to the modeling calculations.

By varying the two transport parameters D_A and V_A and by simultaneously adjusting the incoming flux Γ_0 in the numerical computation, it is attempted to achieve the best agreement between the measured and calculated line radiances. Figure 6 shows the calculated time evolution of the central-chord radiances of the iron-ion resonance lines that is in good agreement with the measured one in Fig. 2(b). In calculating the Fe XXIII radiance, the blending of the Fe XXIII and XX 132-Å lines was taken into account. For the case of Fig. 6, the values of D_A, V_A, and Γ_0 were first chosen in such a way as to simulate the time and amplitude of the Fe XXIV radiance peak and to follow the Fe X radiance evolution; after $t=153$ ms, the time of the termination of ICRF heating, the values were chosen in such a way as to simulate the times of the Fe XVIII and XVI radiance peaks and to reproduce the Fe X radiance. Thus, the curves before 153 ms were obtained with $D_A=100$ cm^2 s^{-1}, $V_A=1200$ cm s^{-1}, and $\Gamma_0=9\times10^{11}$ cm^{-2} s^{-1} until 140 ms and then increasing linearly by a factor of 1.5 in 13 ms; the curves after 153 ms were obtained with $D_A=100$ cm^2 s^{-1}, $V_A=400$ cm s^{-1}, and $\Gamma_0=0$. The following discrepancies still remain between the measured and calculated radiance evolutions. The cal-

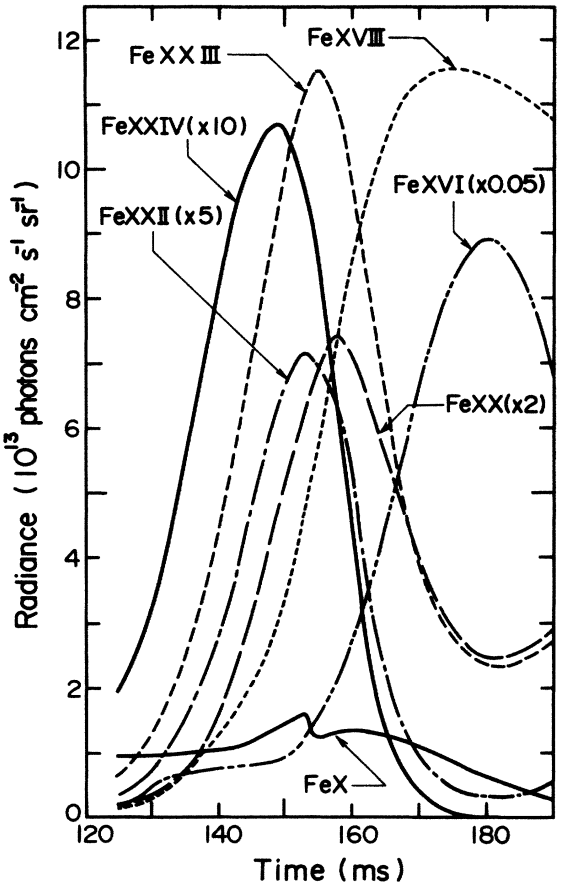

FIG. 6. Calculated time evolution of the central-chord radiances of the iron-ion resonance lines which is compared with the measured one in Fig. 2(b). In calculating the Fe XXIII radiance, the blending of the Fe XXIII and XX 132-Å lines was taken into account. The time-dependent modeling calculations were started at $t=118$ ms, the time of the initiation of ICRF heating which lasts 35 ms from 118 to 153 ms.

culated amplitude of the Fe XXII radiance peak is about a factor of 3 smaller than the measured one; the calculated amplitude of the Fe XVI radiance peak is about a factor of 6 larger than the measured one. The calculated Fe XVIII radiance drop after the peak is too small as compared to the measured one, The Fe X radiance rise and peak after about 160 ms, observed in the experiments, are not well reproduced in the calculations. Otherwise the agreement is quite good.

At present there are various uncertainties in both the experimental measurements and the modeling calculations that tend to make quantitative comparisons tenuous: experimental uncertainties of spectrometer calibration, of plasma shot-to-shot reproducibility, and of electron density and temperature profiles; theoretical uncertainties of the transport model including influx and recycling, and of atomic processes with their rates. In view of these uncertainties and the difficulties in trying to reproduce the signals of different ionization stages perfectly, the overall agreement can be considered satisfactory between the measured and calculated line radiances in Figs. 2(b) and 6. Figure 7 shows the calculated radial profiles of the total iron density n_{Fe} ($=\sum_Z n_Z$) at various times for the case of Fig. 6, giving a picture of large influx and central accumulation of iron. The iron density n_{Fe} increases progressively until $t=153$ ms, the time of the termination of ICRF heating, owing to the large influx Γ_0 of iron which is then transported to the central region by inward convection. Here the convection parameter $S=aV_A/2D_A$,[30] which describes the relative importances of inward convection and diffusion in the iron flux, is very large: $S=138$ before 153 ms and $S=46$ after 153 ms. Diffusion tends to produce flat profiles of n_{Fe}, whereas inward convection tends to produce centrally peaked ones; the dimensionless parameter S gives a measure of the peaking of $n_{Fe}(r)$. The iron density profile $n_{Fe}(r)$ is flat or hollow at first; then $n_{Fe}(r)$ evolves toward a centrally peaked profile as the iron arrives and accumulates in the central region. After 153 ms, the iron continues to accumulate with $\Gamma_0=0$, which is accompanied by a reduction of n_{Fe} near the edge at $r=a$.

At $t>150$ ms, the calculated central iron density $n_{Fe}(0)$ is of the order of 10^{10} cm^{-3}. The corresponding radiated power densities, estimated from the theoretical radiation efficiencies for coronal equilibrium distributions of iron[31,32] and the measured electron densities and temperatures, are much smaller than the measured ones

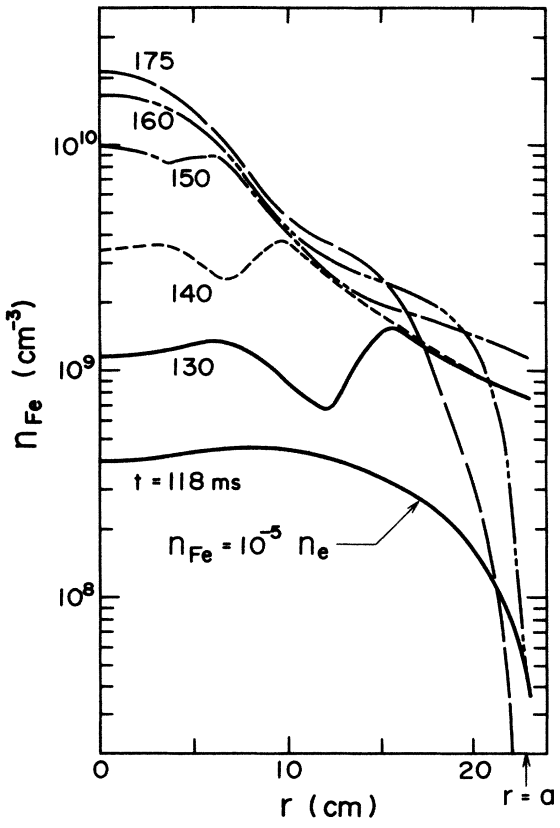

FIG. 7. Calculated radial profiles of the total iron density n_{Fe} ($=\sum_Z n_Z$) at various times for the case of Fig. 6. Here $a=23$ cm is the limiter radius.

$W_{rad}(0)$ in Fig. 4(b). This difference may be due to radiation from titanium, oxygen, and carbon that are the primary intrinsic impurities besides iron in the present experiments. Further improvements in the modeling calculations are now in progress, including the estimation of the radiated power, to clear up the causes of the discrepancies between the measurements and calculations described above.

In conclusion, we have spectroscopically investigated the iron-ion line radiation in the xuv region during ICRF heating experiments in the JIPP T-II-U tokamak. Attention has been focused on the radiation increase during ICRF heating and on the subsequent sequential peaking of the radiation from the highest to the lowest ionization stages. The rf-power injection was accompanied by strong gas puffing and additional current rise, which raised the electron density and concurrently lowered the central electron temperature. The electron-temperature decrease in the central region, which was further promoted by radiative losses due to metallic impurities, continued after ICRF heating. The spectroscopic observations are interpreted as showing that the ICRF heating causes a large additional influx of iron into the plasma, and that the iron accumulates preferentially in the plasma interior with long confinement times. The sequential peaking of the radiation reflects the decrease in the electron temperature and the concurrent recombination into successively lower stages. These interpretations are supported by the soft-x-ray and bolometric measurements, and confirmed by the modeling calculations that reproduce the iron-ion line radiances. Impurity accumulation is not typical of most tokamak experiments; in the present experiments, moreover, impurity levels are relatively low and accumulation is not serious. However, the present results emphasize that a deeper understanding of impurity transport and confinement as well as of impurity generation may be needed for near-future tokamak experiments with higher-power, longer-pulse ICRF heating. Further investigations will be required to reveal the mechanisms responsible for impurity accumulation during ICRF heating[44] as observed in the present experiments.

ACKNOWLEDGMENTS

Three of us (K.O., T.O., and Y.U.) would like to thank Professor J. Fujita and Professor M. Otsuka of Nagoya University and Professor T. Oda of Hiroshima University for providing the opportunity to participate in the JIPP T-II-U ICRF heating experiments. They would also like to thank Dr. M. Iwamoto and Dr. Y. Murai of Mitsubishi Electric Corporation for encouragement during this work.

---

*Present address: Products Development Laboratory, Mitsubishi Electric Corporation, Tsukaguchi-honmachi, Amagasaki 661, Japan.

[1]R. C. Isler, Nucl. Fusion **24**, 1599 (1984).
[2]W. Engelhardt *et al.*, in *Plasma Physics and Controlled Nuclear Fusion Research,* Proceedings of the 7th International Conference, Innsbruck, 1978 (IAEA, Vienna, 1979), Vol. 1, p. 123.
[3]K. Toi *et al.*, Nucl. Fusion **19**, 1643 (1979).
[4]R. C. Isler *et al.*, Phys. Rev. Lett. **47**, 333 (1981).
[5]G. L. Jahns *et al.*, Nucl. Fusion **22**, 1049 (1982).
[6]R. C. Isler *et al.*, Nucl. Fusion **23**, 1017 (1983).
[7]S. Tsuji *et al.*, Nucl. Fusion **25**, 305 (1985).
[8]R. C. Isler *et al.*, Phys. Rev. Lett. **47**, 649 (1981).
[9]R. C. Isler, E. C. Crume, and D. E. Arnurius, Phys. Rev. A **26**, 2105 (1982).
[10]C. E. Bush *et al.*, Nucl. Fusion **23**, 67 (1983).
[11]R. C. Isler, P. D. Morgan, and N. J. Peacock, Nucl. Fusion **25**, 386 (1985).
[12]D. Q. Hwang, G. Grotz, and J. C. Hosea, J. Vac. Sci. Technol. **20**, 1273 (1982).
[13]Equipe TFR, Plasma Phys. **24**, 615 (1982).
[14]S. Suckewer *et al.*, Nucl. Fusion **21**, 981 (1981).
[15]H. Kimura *et al.*, in *Plasma Physics and Controlled Nuclear Fusion Research,* Proceedings of the 9th International Conference, Baltimore, 1982 (IAEA, Vienna, 1983), Vol. 2, p. 113.
[16]Equipe TFR, Plasma Phys. Contr. Fusion **26**, 165 (1984).
[17]B. C. Stratton *et al.*, Nucl. Fusion **24**, 767 (1984).
[18]K. Toi *et al.*, in *Plasma Physics and Controlled Nuclear Fusion Research,* Proceedings of the 10th International Conference, London, 1984 (IAEA, Vienna, 1985), Vol. 1, p. 523.
[19]C. Breton *et al.*, Plasma Phys. Contr. Fusion **27**, 355 (1985).
[20]K. Sato *et al.*, Nucl. Fusion (to be published).
[21]K. Sato, M. Otsuka, and M. Mimura, Appl. Opt. **23**, 3336 (1984).
[22]J. R. Fuhr, G. A. Martin, W. L. Wiese, and S. M. Younger, J. Phys. Chem. Ref. Data **10**, 305 (1981).
[23]TFR Group, Nucl. Fusion **17**, 1297 (1977).
[24]E. Hinnov *et al.*, Nucl. Fusion **18**, 1305 (1978).
[25]J. Fujita *et al.*, in *Plasma Physics and Controlled Nuclear Fusion Research,* Proceedings of the 7th International Conference, Innsbruck, 1978 (IAEA, Vienna, 1979), Vol. 1, p. 247.
[26]R. C. Isler, E. C. Crume, and H. C. Howe, Nucl. Fusion **19**, 727 (1979).
[27]E. Hinnov *et al.*, Nucl. Fusion **22**, 325 (1982).
[28]M. Ichimura *et al.*, Nucl. Fusion **24**, 709 (1984).
[29]R. J. Hawryluk *et al.*, Nucl. Fusion **19**, 1307 (1979).
[30]F. H. Seguin, R. Petrasso, and E. S. Marmar, Phys. Rev. Lett. **51**, 455 (1983).
[31]D. E. Post *et al.*, At. Data Nucl. Data Tables **20**, 397 (1977).
[32]C. Breton, C. De Michelis, and M. Mattioli, J. Quant. Spectrosc. Radiat. Transfer **19**, 367 (1978).
[33]J. Fujita *et al.*, in *Controlled Fusion and Plasma Physics,* Proceedings of the 12th European Conference, Budapest, 1985 (European Physical Society, Budapest, 1985), Vol. 9F, Pt. III, p. 702.
[34]S. Suckewer *et al.*, Nucl. Fusion **24**, 815 (1984).
[35]T. Amano and E. C. Crume, Oak Ridge National Laboratory Report No. ORNL/TM-6363, 1978 (unpublished).
[36]TFR Group, Nucl. Fusion **23**, 559 (1983).
[37]C. Breton *et al.*, J. Phys. B **16**, 2627 (1983).
[38]W. Lotz, Max-Planck-Institut für Plasmaphysik, Garching, Report No. IPP 1/56, 1967 (unpublished); Report No. IPP

1/76, 1968 (unpublished).
[39]R. D. Cowan and J. B. Mann, Astrophys. J. **232**, 940 (1979).
[40]S. von Goeler *et al.*, Nucl. Fusion **15**, 301 (1975).
[41]A. Burgess, Astrophys. J. **141**, 1588 (1965).
[42]H. Van Regemorter, Astrophys. J. **136**, 906 (1962).
[43]R. Mewe, Astron. Astrophys. **20**, 215 (1972).
[44]V. S. Chan, S. C. Chiu, and S. K. Wong, Nucl. Fusion **25**, 697 (1985).